Expanded View Figures

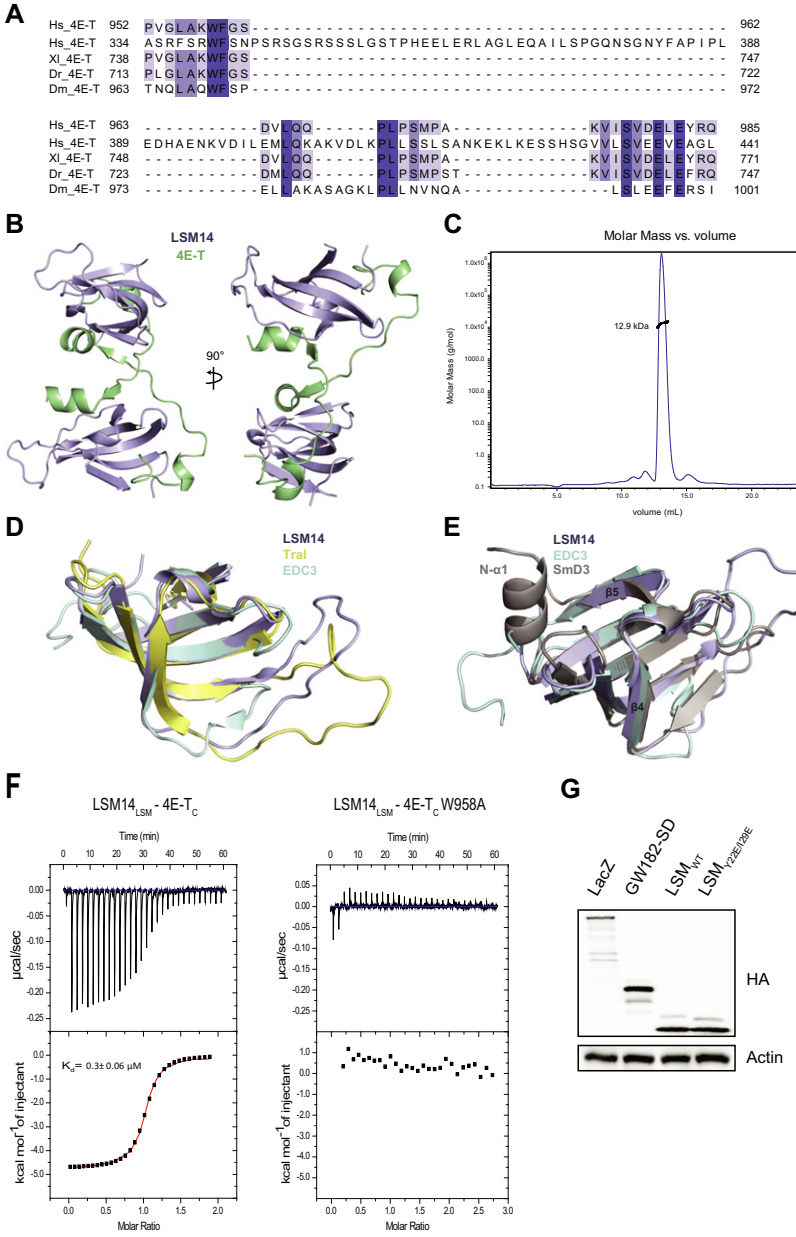

Figure EV1. Structural analysis of the $LSM14_{LSM}$–4E-T_C complex.

A Sequence alignment of conserved amino acids within the C-terminal and middle motifs of human (Hs), *Xenopus laevis* (Xl), zebrafish (Dr), and *Drosophila melanogaster* (Dm) 4E-T proteins.

B Crystal structure of the N-terminal LSM domain of LSM14 in complex with a conserved C-terminal 4E-T fragment reveals a tetrameric complex with 2:2 stoichiometry. Two perpendicular views shown in cartoon representation. Each LSM14 molecule (blue) is simultaneously bound by two 4E-T molecules (green).

C Analysis of purified $LSM14_{LSM}$–4E-T_C complex by size exclusion chromatography coupled to MALS. The molar mass distribution (left ordinate, black line) indicates a molar mass of 12.9 kDa, which corresponds to a 1:1 complex in solution.

D Structural comparison of the LSM domains of human LSM14 (blue), *Drosophila* Tral (yellow), and human EDC3 (cyan). The structures were superimposed using the DALI server (Holm & Laakso, 2016) and are shown in identical orientation.

E Structural comparison of the LSM domains of human LSM14 (blue), human EDC3 (cyan), and human SmD3 (gray, PDB ID: 1D3B-A). The structures were superimposed using the DALI server (Holm & Laakso, 2016) and are shown in identical orientation.

F ITC binding isotherms of 500 µM 4E-T_C peptide (left) and a W958A mutant (right) titrated into 50 µM $LSM14_{LSM}$. Data were fitted to a single-binding site model, and the dissociation constant (K_d) was determined based on three independent experiments. Data analysis, fitting, and K_d calculation were performed using Origin7.

G Representative Western blot analysis of expressed λNHA-tagged proteins showing comparable expression of the respective proteins. Proteins were resolved by SDS–PAGE and probed with HA and actin antibodies.

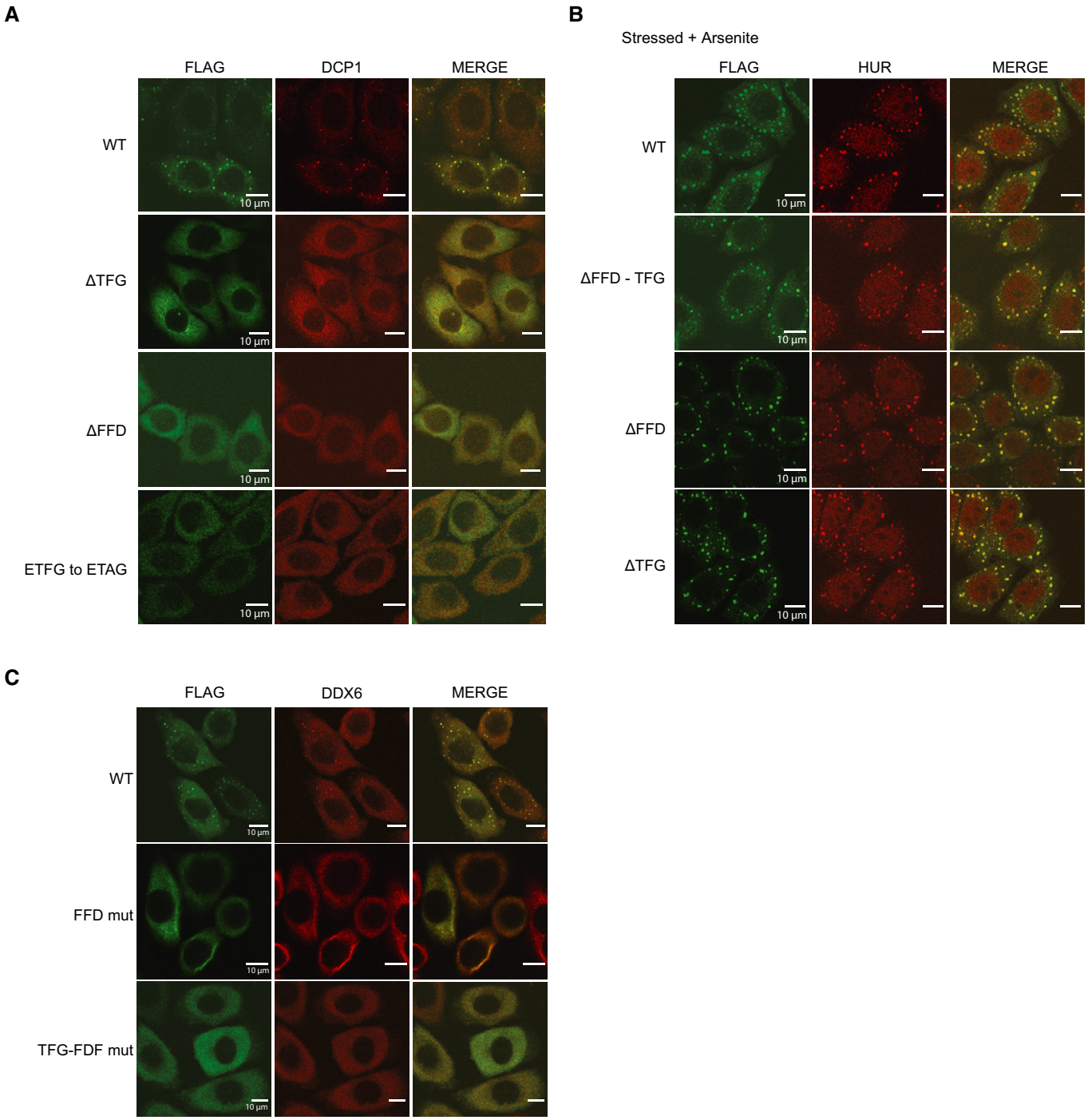

Figure EV2. LSM14-dependent RNP granule assembly.

A Confocal fluorescence micrographs of fixed HeLa cells expressing FLAG-fusions of full-length LSM14 (WT) and mutant proteins. Cells were stained with anti-FLAG (green) and anti-DCP1 (red) antibodies. While WT LSM14 leads to formation of distinct cytoplasmic foci (P-bodies), indicated deletion and substitution variants of LSM14 impair assembly of P-bodies.

B Confocal fluorescence micrographs of arsenite-induced stress granule formation in fixed HeLa cells expressing FLAG-fusions of full-length LSM14 (WT) and mutant proteins. Cells were stained with anti-FLAG (green) and anti-HUR (HUR, Hu protein R, red) antibodies. All tested LSM14 mutants are recruited to stress granules independently of their ability to bind DDX6 or EDC4.

C Confocal fluorescence micrographs of fixed HeLa cells expressing FLAG-fusions of full-length LSM14 (WT) and mutant proteins. Cells were stained with anti-FLAG (green) and anti-DDX6 (red) antibodies. While WT LSM14 leads to formation of distinct cytoplasmic foci (P-bodies), inversion of the FDF and TFG motifs in LSM14 impairs P-body assembly.

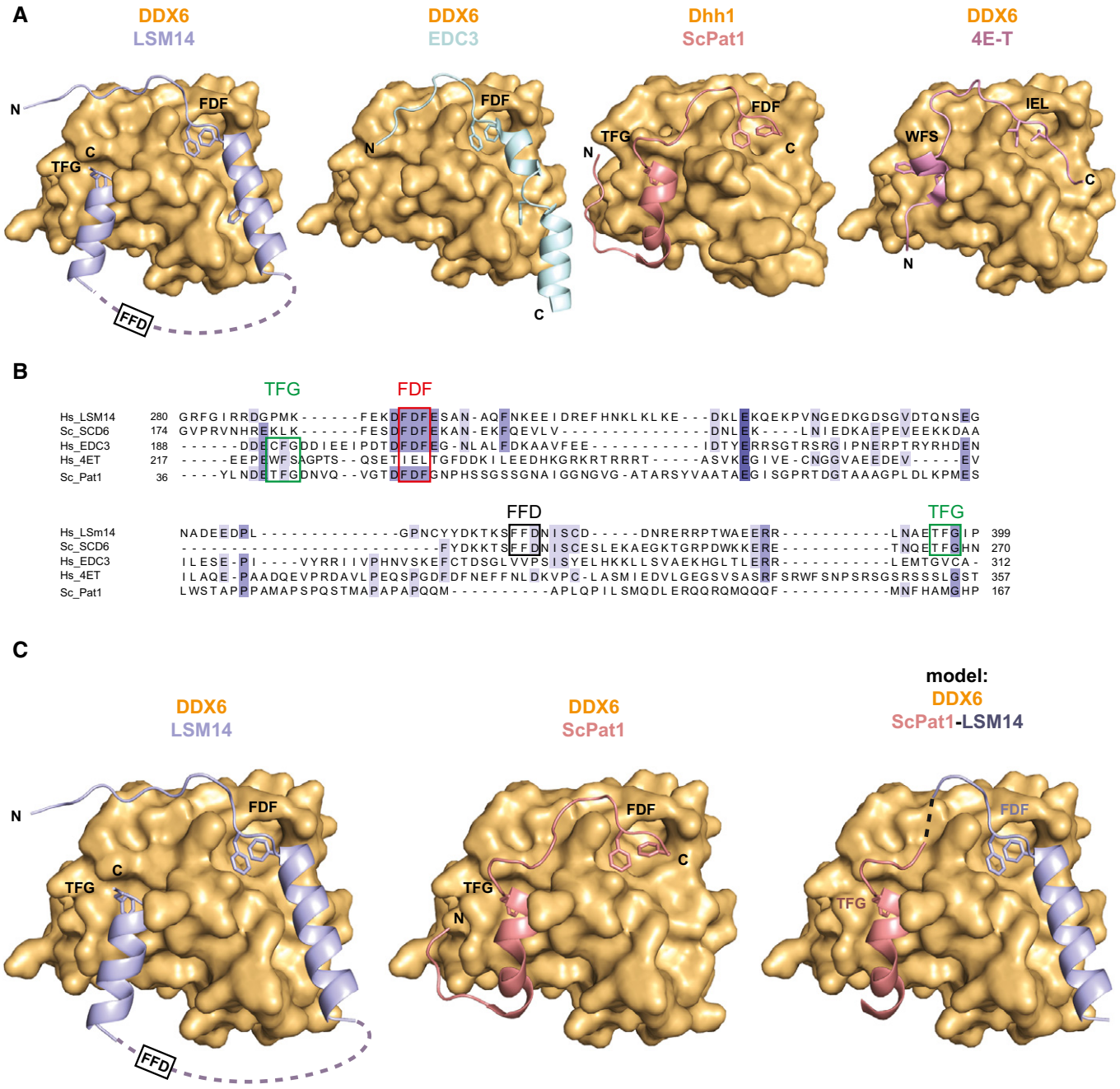

Figure EV3. Hydrophobic surfaces on DDX6$_C$ mediate interactions with conserved sequence motifs in EDC3, PATL1, 4E-T, and LSM14.

A Side-by-side structural comparison of human DDX6$_C$ or its yeast homolog Dhh1 (orange) in complexes with LSM14 (blue), EDC3 (cyan, PDB ID 2WAY), yeast (Sc) Pat1 (salmon, PDB ID 4BRW), and 4E-T (pink, PDB ID 5ANR). Structures are shown in identical orientations, and conserved sequence motifs are indicated. Unstructured portion of the LSM14 polypeptide chain is depicted as dashed line. Conserved sequence motifs from the DDX6-interacting factors occupy identical patches on the surface of DDX6, yet the topology of these motifs is different in LSM14.

B Sequence alignment of regions encompassing the FDF (red box), FFD (black box), and TFG (green boxes) motifs in human (Hs) LSM14, yeast (Sc) SCD6, human EDC3, and 4E-T and yeast Pat1.

C Structural model of the Pat1-LSM14 chimeric protein used in this study, colored as in (B). Left: Structure of LSM14$_{FDF\text{-}TFG}$ in complex with DDX6$_C$. Middle: Model of yeast Pat1 FDF-TFG motifs (salmon, PDB ID 4BRW) bound to human DDX6$_C$. Right: Model of a Pat1-LSM14 chimeric protein in complex with DDX6$_C$. Fusion of a Pat1-fragment containing the TFG motif upstream of a LSM14-fragment containing the FDF motif is indicated by black dashed line. Motifs mediating interaction with DDX6 are indicated.

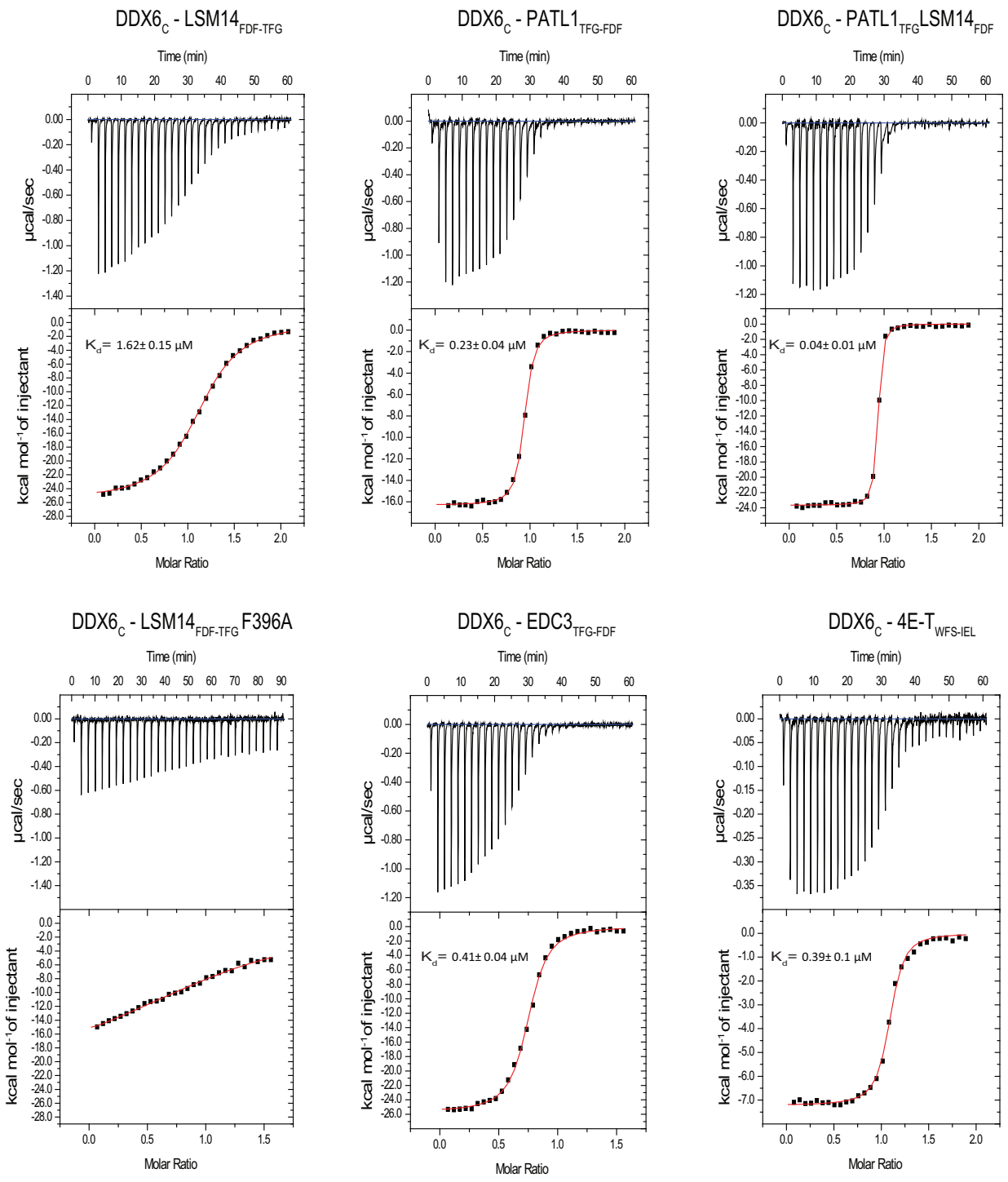

Figure EV4. ITC analysis of DDX6$_C$ binding by LSM14, PATL1, EDC3, and 4E-T.

ITC binding isotherms of 500 µM LSM14$_{FDF-TFG}$ (upper left), PATL1$_{TFG-FDF}$ (upper middle), PATL1$_{TFG}$LSM14$_{FDF}$ (upper right), LSM14$_{FDF-TFG}$ F396A (lower left), MBP-EDC3$_{TFG-FDF}$ (lower middle), and 4E-T$_{WFS-IEL}$ (lower right) titrated into 50 µM DDX6$_C$. Data were fitted to a single-binding site model, and the dissociation constants (K_d) were determined based on three independent experiments. Data analysis, fitting, and K_d calculation were performed using Origin7.

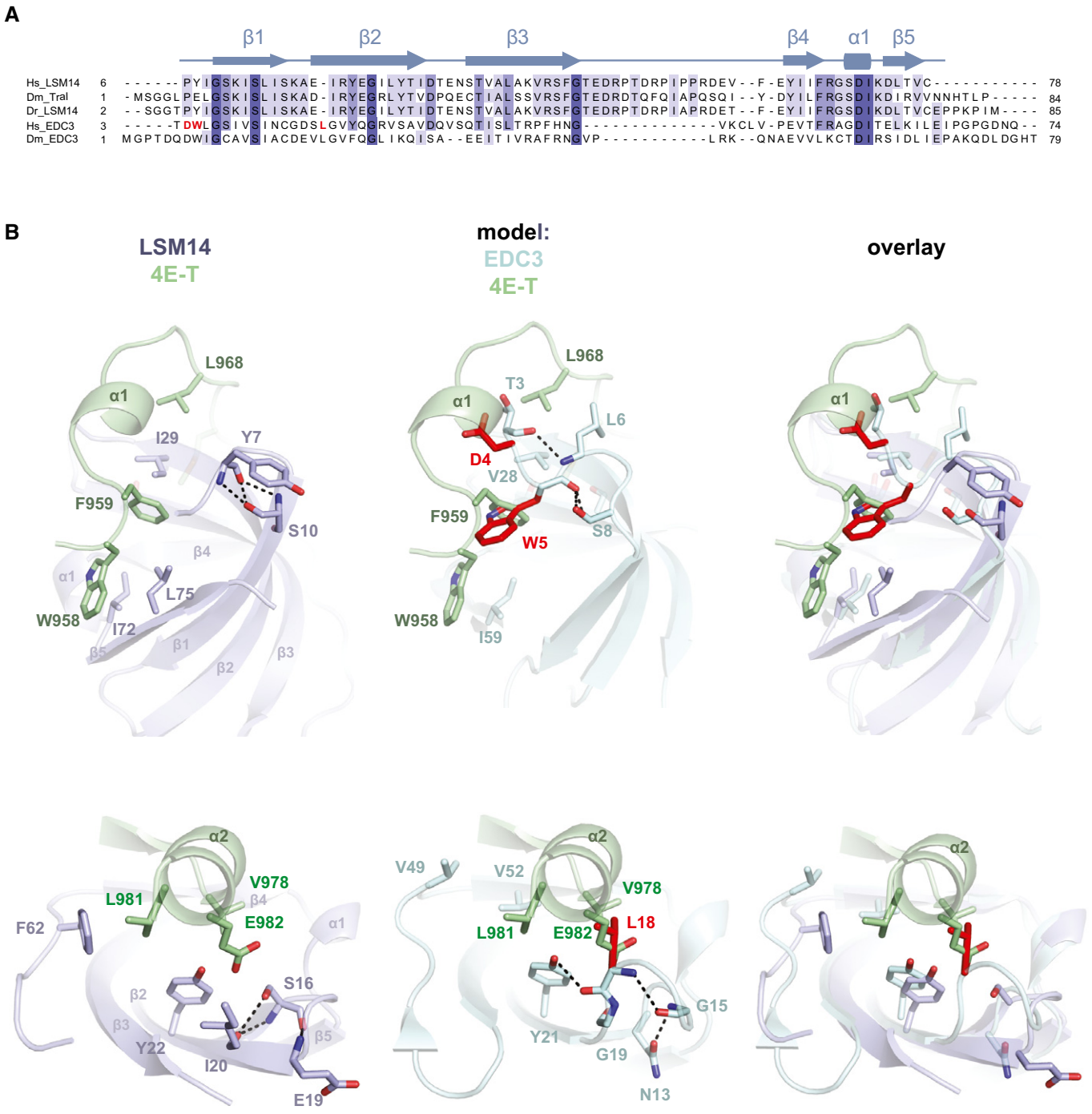

Figure EV5. Structural comparison of the LSM domains of LSM14 and EDC3 in the context of 4E-T binding.

A Multiple sequence alignment of the LSM domains of human (Hs) LSM14, *Drosophila* (Dm) Tral, zebrafish (Dr) LSM14, human (Hs) and *Drosophila* (Dm) EDC3. Residues of EDC3 that would impair 4E-T binding by steric clashes are colored in red.

B Structural comparison of the LSM14–4E-T complex with a model of the EDC3–4E-T complex. Left: Zoomed-in view of two main interactions interfaces between LSM14 (light blue) and 4E-T (green). Middle: Model of the LSM domain of EDC3 (cyan, PDB ID 2VC8) superimposed with the LSM14-binding motifs of 4E-T, shown in identical orientations as LSM14. Right: Overlay of the LSM14 and EDC3 LSM domains, shown in the respective orientations. 4E-T residues involved in complex formation are shown as sticks and labeled by single letter code. Residues from LSM14 and EDC3 involved in complex formation or intramolecular interactions are shown as sticks and labeled by single letter code. EDC3 residues clashing with 4E-T are colored in red. Hydrogen-bonding interactions mediating divergent structural features in the LSM14 and EDC3 LSM domains are indicated with black dashed lines. Secondary structure elements are numbered as in Fig 2A.